J Nanopart Res (2022) 24: 79
https://doi.org/10.1007/s11051-022-05445-z

RESEARCH PAPER

The effect of the body wake and operator motion on the containment of nanometer-scale airborne substances using a conventional fume hood and specially designed enclosing hood: a comparison using computational fluid dynamics

Chen Shen · Kevin H. Dunn · Susan R. Woskie · James S. Bennett · Michael J. Ellenbecker · David S. Dandy · Candace Su-Jung Tsai

Received: 3 June 2021 / Accepted: 22 February 2022 / Published online: 9 April 2022

Abstract Airborne substances in the nanoparticle size range would mostly follow the primary airflow patterns, which emphasizes the importance of understanding the airflow dynamics to effectively control exposures to toxic airborne substances such as nanometer-sized particles. Chemical fume hoods are being utilized as primary controls for worker exposure to airborne substances including nanometer-scale materials due to their overall availability and history of effective contaminant. This study evaluates the impact of the body wake on the containment performance of a conventional constant air volume (CAV) and a new "nano" ventilated enclosing hood using numerical methods. Numerical studies have been performed to predict leaks of nanomaterials handled inside the hood. We further performed experiments in this study to validate the velocity fields predicted by the computational fluid dynamic (CFD) models and to provide a basis for evaluating the impact of the human body on fume hood containment performance. Using these validated models, the effects of the motion of the arms moving out of the hood were simulated using CFD to assess how one of the common actions of an operator/user may affect containment. Results of our simulations show that areas near the hood side airfoils and directly behind the sash are more likely to concentrate contaminants released inside the hood and potentially result in leakage based on internal airflow patterns. These areas are key to monitor when assessing fume hood containment along with the operator/mannequin breathing zone to get an understanding of potential leak areas which might contribute to operator exposure as well as exposure to others inside the laboratory.

Keywords Nanoparticle · Fume hood · Containment · CFD

Candace Su-Jung Tsai is the project Principal Investigator of a contract with the US National Institute for Occupational Safety and Health.

C. Shen (✉) · D. S. Dandy · C. S.-J. Tsai
Department of Chemical and Biological Engineering, College of Engineering, Colorado State University, Fort Collins, CO, USA
e-mail: chenshen@rams.colostate.edu

K. H. Dunn (✉) · J. S. Bennett
Engineering and Physical Hazards Branch, Division of Applied Research and Technology, National Institute for Occupational Safety and Health, Cincinnati, OH, USA
e-mail: KDunn@cdc.gov

S. R. Woskie · M. J. Ellenbecker
Department of Work Environment, College of Health Sciences, University of Massachusetts Lowell, Lowell, MA, USA

C. S.-J. Tsai
Department of Environmental Health Sciences, Fielding School of Public Health, University of California Los Angeles, Los Angeles, CA, USA

Introduction

It is desirable when working with nanometer-scale airborne materials, including engineered nanomaterials whose agglomerated sizes are within a few hundred nanometers, to employ effective exposure controls and proper work practices so that exposure and subsequent adverse effects on process performance are minimized and a safe and healthy work environment is maintained (Bavasso et al. 2016; NIOSH 2009). Airborne substances smaller than one micrometer in size would mostly follow airflow pattern and flow in the airstream (Hinds 1999). This property emphasizes the importance of understanding the airflow dynamics to further manage the control measures to toxic airborne substances such as nanometer-sized particles (Ong et al. 2020; Asadi et al. 2020). Chemical fume hoods are being utilized as primary controls for worker exposure to airborne substances including nanometer-scale materials due to their overall availability and history of effective contaminant (Ding et al. 2017). However, traditional designs for laboratory fume hoods create airflow patterns that form recirculation regions inside the hood. In addition, airflow around the worker creates a negative pressure region downstream of the worker that may provide a mechanism for transporting contaminants out of the hood and into the breathing zone of the worker (Flynn and Ljungqvist 1995a). This study utilized computational fluid dynamics (CFD) to assess the impacts of the presence of the worker body and the motion of the arms on the containment effectiveness of a traditional constant air volume (CAV) fume hood and a ventilated enclosure that is designed for handling nanomaterials.

The use of visualization techniques has proved critical in gaining a better understanding of the flow patterns which affect overall hood performance (Tsai 2013; Huang et al. 2007a; Tseng et al. 2006; Varley and Ghorashi 1997). Several researchers have identified the existence of an airflow pattern inside the hood that carries contaminants released above the work surface into a large recirculation zone located behind the sash (Tseng et al. 2006, 2010; Ljungqvist 1991; Hu et al. 1996, 1998; Nicholson et al. 2000; Lan and Viswanathan 2001a; Ivany et al. 1989). This recirculation region acts to trap contaminants and is potentially a problematic area for leakage of contaminants generated inside the hood. In addition, boundary layer separation produces a wake region, characterized by eddies or vortices that entrain air into a reverse-flow region near the body (Flynn and Ljungqvist 1995b; Kim and Flynn 1992, 1991a, b; George et al. 1990). This near-wake region may serve to transport contaminants from the fume hood into the breathing zone of the person standing in front of the hood.

Kim and Flynn (1991) showed that a recirculation region forms downstream of a worker in a free stream (as air flows from the back of the worker) with a length proportional to the mannequin's shoulder width (Kim and Flynn 1991a). Their research also indicated that a vertical flow field was present downstream near the worker where the mean flow field would serve to transport contaminants from the waist level or higher into the breathing zone. Further research by Kim and Flynn (1991) confirmed that this recirculation region could transport contaminants released downstream of the worker into the breathing zone (Kim and Flynn 1991b). Welling et al. (2000) evaluated a range of conditions related to potential exposure of a mannequin in free stream including body heat, arm motion, variations in air velocity and body orientation (Welling et al. 2000). This research observed lower breathing zone concentrations for a mannequin at lower free stream velocities than at higher velocities; and the effect of arm motion was likened to a fan that disrupted airflows and resulted in increased contaminant dispersion upward. Upstream disruptions that interfere with near-wake eddy formation and maintenance have also been explored as a contaminant control measure (Bennett et al. 2003). Other researchers have also identified significant fume hood leaks when the operator moved their arms in and out of the hood, a common practice used to move objects and equipment in and out of the hood or upon completion of work (DiBerardinis et al. 1991a; Mosovsky 1995).

In an experimental study, the presence of a mannequin was shown to interact with the regions of airflow separation near the bottom and sides of the hood to increase the size of the recirculation region near the doorsill and side poles than without the mannequin (Tseng et al. 2007). The presence of the mannequin increased the intensity and size of the separation and recirculation zones around the middle and lower levels of the hood opening. These effects resulted in fume hood leaks at the middle and lower levels hood opening being more likely than without the

mannequin. A meta-analysis of 43 published experimental fume hood containment studies was conducted to identify the important elements that affect the performance of a laboratory fume hood (Ahn et al. 2008). This analysis showed that the presence of a mannequin/human subject in front of the hood caused the greatest risk of containment failure among all factors evaluated, resulting in a 199% higher risk of hood failure than when no mannequin was present.

The impacts of the body on fume hood containment have also been evaluated using CFD. CFD is a useful tool and has been used in several previous studies to evaluate the impact of hood design on containment performance (Hu et al. 1996, 1998; Nicholson et al. 2000; Lan and Viswanathan 2001a, b; Braconnier and Bonthoux 2010). These studies have led to a better understanding of how design factors affect performance and have improved hood containment. Hu et al. used 2-D CFD models to look at several different design configurations including the inclusion of a sash handle, the effect of interior baffles and a louvered bypass on hood airflow characteristics (Hu et al. 1996, 1998). They found that the design and placement of the sash handle has important consequences on the likelihood of contaminant leakage around the bottom of the sash. This effect is due to the impact of turbulence caused by the handle which causes contaminants caught in the large recirculation region behind the hood sash to leak out of the hood. Nicholson et al. (2000) developed a 3-D model which included a rear baffle and an aerodynamic lipfoil (located at the base of the fume hood opening) (Nicholson et al. 2000). The simulations showed that removing the rear baffle eliminated the flow across the hood floor, increased the size of the vortex behind the sash and created a large stagnant zone at the back of the work surface. With full aerodynamic features (baffle and lipfoil), the face velocity across the opening was uniform and containment performance was dramatically improved. Because of these and other studies, most of these features are commonly found on chemical fume hoods today. Kumula et al. (1996) evaluated the effect on exposure of the recirculation region downstream of the worker using both experimental and CFD methods (Kulmala et al. 1996). Experimental results showed that the mean recirculation region length did not greatly depend on free stream velocity and appeared to be 1.5 times the mannequin's width. A clockwise upward recirculation region existed above the mannequin hip level which provided transport to the breathing zone consistent with the findings from other researchers. Braconnier and Bonthoux (2010) evaluated a type II microbiological safety cabinet (BSC) (called a cytotoxic safety cabinet) using a 3-D CFD model (Braconnier and Bonthoux 2010). The BSC differs from a standard fume hood in that there is an exhaust slot along the front of the hood at the base and a continuous down flow inside the hood which is recirculated from the overall exhaust flow following high efficiency particulate air (HEPA) filtration. A blockage representing an operator in front of the hood caused a small wake in front of the mannequin. In addition, there was a reduction in the inward air velocity at mid opening heights; but it did not cause air to flow out of the hood. Further, a simplified arm geometry (without a body) similar to one used for BSC containment testing was evaluated and found not to have a significant effect on containment (Braconnier and Bonthoux 2010). No fume hood CFD studies found in the published literature have evaluated the impact of user motion on containment effectiveness.

Nano hoods specifically designed for nanomaterials have been manufactured based on low turbulence balance enclosures which were initially developed for the weighing of pharmaceutical powders. Bench-mounted weighing enclosures are commonly used for the manipulation of small amounts of material. These fume hood-like local exhaust ventilation devices typically operate at airflows lower than those in traditional fume hoods and use airfoils at enclosure sills to reduce turbulence and potential for leakage. New lower flow hoods are being marketed and used for the manipulation of nanomaterials. The use of lower inlet airflows may reduce the impact of turbulence and the body wake on the potential for fume hood leakage. However, there is little information on their performance.

This study used numerical methods to evaluate the impact of the body wake on containment performance of a CAV and the nano hood. Previous experimental studies presented hood leakages with nanomaterials handled inside the hood (Dunn et al. 2014; Tsai et al. 2009). We performed experiments in the current study to validate the CFD models and to provide a basis for evaluating the impact of the human body on fume hood containment performance. Thus, the effects of arm motion into and out of the hood was

simulated using CFD in this study to assess how one of the common actions of an operator/user may affect containment.

Methods

Description of hoods and equipment setup

The "nano" ventilated enclosing hood evaluated was the A1 Safetech ST1 (Dusseldorf, Germany) potent powder weighing enclosure (hereafter referred to as the nano hood). The exhaust of the hood is routed through an attached fan and HEPA filtration unit with air recirculated into the room. The HEPA fan/filter unit provides the important function for the removal of powders and filtration of air prior to recirculating the air to the workplace. The HEPA fan/filter unit (33 cm in width × 33 cm in depth × 50 cm in height) was co-located to the right of the hood face. This hood located in a university lab was 7.32 m in width by 4.85 m in depth with a ceiling height of 2.75 m. The hood was located on a bench top with shelving located above the hood along with an assortment of lab equipment (see Fig. 1a). More details on these hoods as well as the laboratory spaces are discussed in a previous study by Dunn et al. (2014).

The traditional fume hood evaluated in this study was the Safety-Flow Laboratory Fume Hood, Model 93-509Q (Fisher Scientific, Pittsburgh, PA). This type of fume hood is known as a constant air volume hood which maintains a uniform volumetric exhaust flow (hereafter referred to as the CAV hood). The hood was located on a bench top adjacent to an atomic absorption spectrophotometer and lab sink. The hood dimensions are 62 cm (height) × 130 cm (width) × 68 cm (depth). This hood was located in a university lab, 7.3 m wide by 5.8 m deep and with a ceiling height of 2.8 m (see Fig. 1b). The hood was exhausted out of the room through a facility exhaust system.

The mannequin used for the experiments was the upper body of a standard mannequin mounted on a wooden platform as shown in Fig. 1a. This mannequin had a shoulder width of 42 cm with a shoulder height of 140 cm and a total height of 164 cm above the floor. The mannequin head dimensions were 16 cm from back of head to nose tip and 16 cm across the head (from ear to ear). The body of the mannequin was placed at a distance of 5 cm from the inlet airfoil of the nano hood. When using the CAV hood, the body of the mannequin was placed directly against the inlet airfoil with the nose distance to the sash of approximately 10 cm. The distance between the mannequin and the CAV hood sash was set by the ASHRAE test method (ASHRAE 2016). For the nano hood, it was set based on the physical limitations for positioning the mannequin close to the hood opening. The difference in geometry between these two hoods does not allow for the distance to be consistent.

Numerical model details

Airflow and contaminant dispersion simulations were conducted using ANSYS/Fluent version 16.1.0, a commercially available CFD code (Ansys, Canonsburg, PA). The hood and surrounding details were modeled to account for the impact of furniture and lab equipment on airflow patterns. The mannequin was simulated in the CFD model as a block structure with the following dimensions: head: 16 cm × 16 cm × 32 cm; legs: 12 cm × 12 cm; arms: 8 cm × 8 cm; shoulder width: 43 cm; shoulder height: 142 cm; body depth: 20 cm, and; torso length: 70 cm. For the base model case, the arms were positioned at the side of the torso consistent with the experimental conditions. When simulating arm motion, the arms were placed inside the hood.

The furniture and lab equipment were modeled as well to account for the impact of obstacles on the flow field. Hexahedron-dominated meshes were created for low element distortion and skewness. The hood and the room were meshed separately and then merged in ANSYS/Fluent and the contact face of the two mesh was modeled as interface where two regions were mapped. The meshes were more densely packed inside the hood in the vicinity of important geometrical features such as hood inlet, airfoils, and baffle plates for both the CAV and nano hoods. The meshes were coarser outside of the hood and further away from the hood face where flow features were less likely to impact flow patterns inside the hood.

In addition, the grid convergence was evaluated by the development of several grids and the inspection of the solution at key parameters. Grid convergence was assessed on grids ranging from 213,089 cells for CAV Hood to 277,757 cells for nano hood for the coarse grid; further ranging from 3,770,115

Fig. 1 Mannequin and hood setup for experiments. a) Nano hood. b) CAV hood

cells for CAV Hood to 4,007,074 cells for nano hood for the fine grid. The grids were refined by increasing the number of cells in areas of interest including at the hood wall boundaries and surrounding the body form.

A gas tracer source of sulfur hexafluoride (SF_6) was positioned inside the hoods for all simulations to evaluate the dispersion pattern of contaminant gas released inside the hood and the containment for both hood designs. A small cylindrical tracer gas source

with a mass flow of 0.26 ml/min of SF_6 (species mass fraction of 0.13%) was used for the nano hood simulations, while a mass flow of 0.79 ml/min (species mass fraction of 0.40%) was used for the CAV hood. The wall across from the hood face was modeled as a pressure outlet, being set to zero gauge pressure (one atmosphere); flow through pressure boundaries was determined through the CFD solution process. The exhaust boundary condition was established by measuring total hood exhaust flow and imposing this volumetric flow on the exhaust duct as a velocity inlet. The hood exhaust boundary condition was the only source of air movement specified a priori. A summary of key boundary conditions is shown in Table 1.

All simulations discussed in this paper were single phase, steady state, isothermal, and incompressible. A second order upwind spatial discretization scheme was used for model parameters including momentum, turbulent energy and dissipation and a third-order MUSCL discretization scheme was used for species transportation. The least squares cell-based discretization scheme was used for gradient terms and the enhanced wall treatment method was used to accurately capture the flow field near the wall boundaries. The solution process was iterated until the normalized residuals for each conservation equation were less than 10^{-3} for all parameters including velocity components, turbulent kinetic energy and dissipation, pressure and species.

The realizable k-ε turbulence closure model was used as

$$\frac{\partial}{\partial t}(\rho k)+\frac{\partial}{\partial x_j}\left(\rho k u_j\right)=\frac{\partial}{\partial x_j}\left[\left(\mu+\frac{\mu_t}{\sigma_k}\right)\frac{\partial k}{\partial x_j}\right]+\mu_t S^2-\rho\varepsilon \tag{1}$$

$$\frac{\partial}{\partial t}(\rho\varepsilon)+\frac{\partial}{\partial x_j}\left(\rho\varepsilon u_j\right)=\frac{\partial}{\partial x_j}\left[\left(\mu+\frac{\mu_t}{\sigma_\varepsilon}\right)\frac{\partial \varepsilon}{\partial x_j}\right]+\rho C_1 S\varepsilon-\rho C_2\frac{\varepsilon^2}{k+\sqrt{v\varepsilon}} \tag{2}$$

where k is turbulent kinetic energy, ε is the turbulence dissipation rate, t is the time variable, ρ is the density of the fluid, u_j is the mean component of the velocity in the direction x_j, and

$$C_1=\max[0.43,\frac{\eta}{\eta+5}] \tag{3}$$

$$\eta=S\frac{k}{\varepsilon} \tag{4}$$

$$S=\sqrt{2S_{ij}S_{ij}} \tag{5}$$

where S_{ij} is the mean strain-rate tensor and is defined as

$$S_{ij}=\frac{1}{2}(\frac{\partial u_i}{\partial x_j}+\frac{\partial u_j}{\partial x_i}) \tag{6}$$

The default values of the constants for this turbulence model were applied ($C_2=1.9$, $\sigma_k=1.0$, $\sigma_e=1.2$).

Lagrangian particle tracking was used to provide a better understanding of the transport mechanisms which may lead to operator exposure. The Lagrangian particle tracking predicts the trajectories of the particles by solving the equation of motion:

$$\frac{d\boldsymbol{u}_p}{dt}=F_D\left(\boldsymbol{u}-\boldsymbol{u}_p\right)+\frac{\boldsymbol{g}(\rho_p-\rho)}{\rho_p}+\boldsymbol{F} \tag{7}$$

where F_D is the drag force coefficient, $\boldsymbol{u}_p$ is the velocity vector for particles, $\boldsymbol{u}$ is the fluid velocity vector, ρ is the fluid density, ρ_p is the particle density, *and* $\boldsymbol{F}$

Table 1 Boundary conditions used in the simulations

	CAV Hood	Nano Hood
Averaged Mesh cells	5,296,094	3,150,528
Exhaust velocity	7.13 m/s Turbulent Intensity = 10%, Hydraulic Diameter = 0.275 m	7.11 m/s Turbulent Intensity = 10%, Hydraulic Diameter = 0.1 m
Room Inlet	Gauge Total Pressure = 0 pa Turbulent Intensity = 10% Turbulent Viscosity Ratio = 10	Gauge Total Pressure = 0 pa Turbulent Intensity = 10% Turbulent Viscosity Ratio = 10
SF_6	Diffuser velocity = 2.0417e-5 Turbulent Intensity = 10% Turbulent Viscosity Ratio = 10	Diffuser velocity = 2.0417e-5 Turbulent Intensity = 10% Turbulent Viscosity Ratio = 10

is the acceleration term due to additional forces. The drag force coefficient F_D is defined as

$$F_D = \frac{18\mu}{\rho_p d_p^2}\frac{C_D Re}{24} \quad (8)$$

where d_p is the particle diameter, μ is the molecular viscosity of the fluid, and Re is the relative Reynolds number. The shape of particles is approximated as spherical and thus the spherical drag law was applied to calculate C_D.

The Fluent Discrete Phase Model (DPM) served to calculate the paths of nanometer-sized (50 nm) particles to provide insight on factors that affect exposure, both in the traditional fume hood and in the nano hood. To accurately predict particle trajectories under the influence of turbulent flow, Fluent uses a stochastic tracking model (ANSYS 2009). This model allows for a more detailed look at the potential impact of flow patterns on particle dispersion and leaks from the hoods. For these models, the impact of Brownian motion has been calculated and included in the simulations. To assess the impact of operator motion during CFD simulations, the arms were positioned inside of the cabinet near the contaminant source.

The action of pulling arms from the cabinet was simulated using the moving wall boundary condition on the arm boundaries. This condition is implemented in the steady state model by a moving wall boundary condition on cells that define the arm surfaces, which then imparts the velocity to the adjacent air flow, via the no-slip condition. The impact of the motion was evaluated by releasing 50 nm diameter particles from a 10-cm diameter sphere whose center was located inside and 15 cm from the face of each hood. The diameter of 50 nm was chosen based on the medium size of the spherical nanoparticles with defined diameter of 100 nm or smaller. These simulations were conducted using the DPM with the release spheres located in 3 different positions: 1) at the center of the hood; 2) 10 cm from the left side of the hood; and 3) 10 cm from the right side of the hood. These simulations were conducted with arm removal velocities of 0.5, 1.25, and 2.5 m/s. The fate of the particles was evaluated to assess the number of particles escaping the influence of the hood. A grouping of 56,590 particles was released from the sphere to evaluate containment performance.

Experimental validation of hood face velocity

Experimental data were collected to allow for CFD model validation. Airflow measurements were taken to characterize the inlet air flow profile at the face of the fume hoods. A traverse of the hood face with a hot wire anemometer was conducted to evaluate the spatial and temporal variation in air velocities entering the hood. The air velocity measurements were collected using a TSI model 8360 thermal anemometer (Shoreview, MN) with a range of 0.15 to 50 m/s, an accuracy of 3% of reading or 0.02 m/s and a response time of 200 ms (ms) (to 63% of final value). These measurements were conducted both with and without a mannequin in place and with the hood free of clutter and internal obstructions. For the enclosing nano hood, the velocity profile was measured at the mid-plane of the hood face—at a distance of 8.5 cm from the hood base. For the CAV hood, two velocity profiles were conducted at the sash design height of 45 cm. This hood face traverse was conducted at 33% of the sash opening height which was 15 cm above the hood base.

Results and analyses

Model verification and validation

The models were validated by comparing numerical predictions to experimental results, including comparison of both the hood face velocities as shown in Fig. 2. For both hoods, the change in solution parameters was minimal with increasing cell number, and both solutions are shown in the comparison of experimental and CFD results in this section. To allow for comparison of results, the overall grid density and count were kept similar between different hood CFD models. The face velocities of the nano hood were taken at an exhaust airflow of 3.40 m^3/min and ranged from 0.34 to 0.37 m/s across the face of the hood without the mannequin and 0.25–0.44 m/s with the mannequin in place. With the mannequin in place, the midplane velocity dropped significantly in front of the mannequin in the stagnation region downstream of the body for both hoods as presented in Fig. 2a.

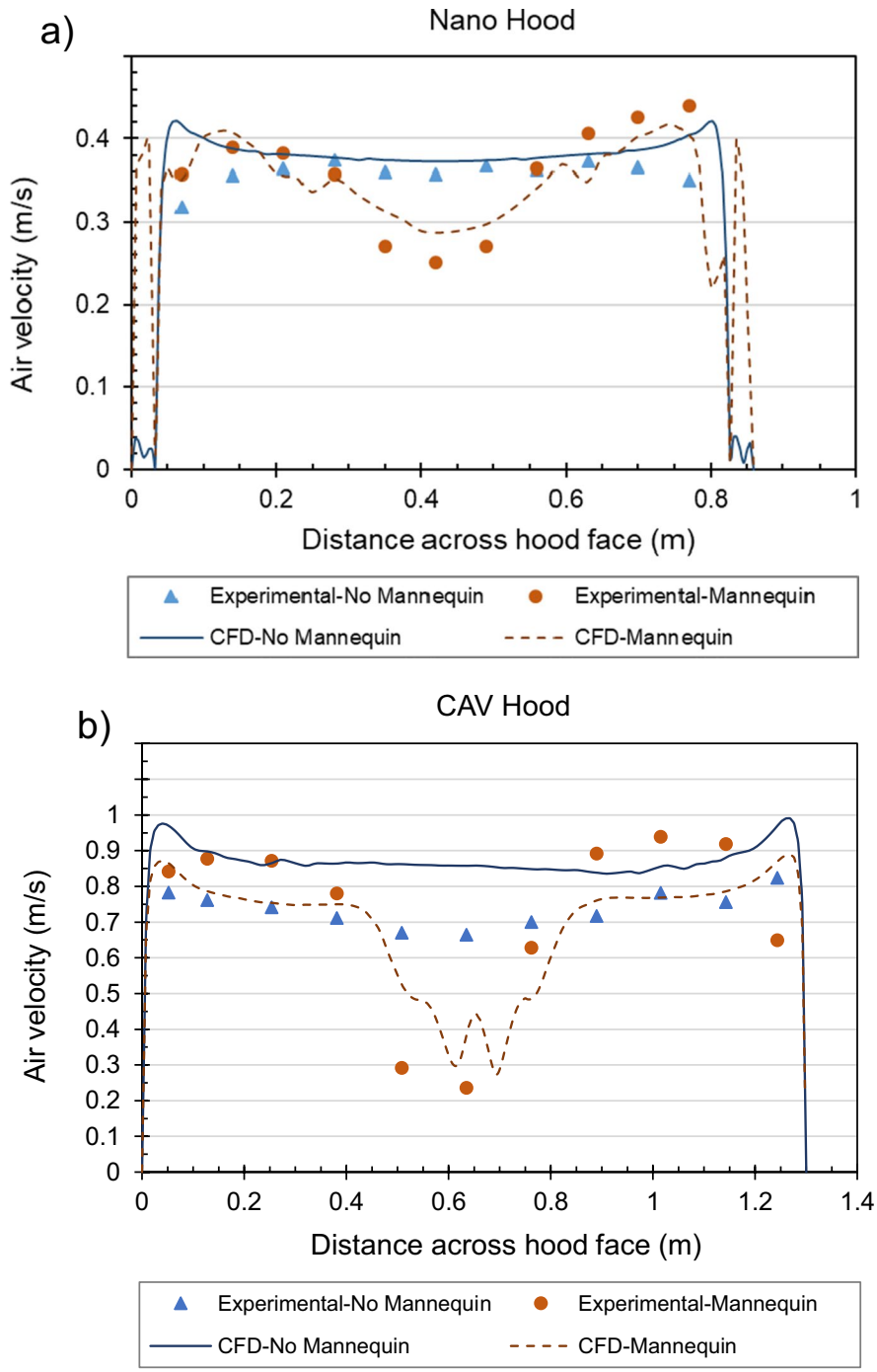

Fig. 2 Comparison of velocity profile with CFD predictions for the a) nano hood at midplane of the opening and b) the CAV hood at 33% of sash opening (15 cm)

The root mean square (RMS) differences between the experimental measurements and analytical predictions for the face velocities were approximately 11% for the nano hood without the mannequin and 24% for the nano hood with the mannequin in place.

For the CAV hood, the average face velocity at 33% of the sash height (15 cm) ranged in 0.66–0.82 m/s without the mannequin and 0.23–0.91 m/s with the mannequin in place as presented in Fig. 2b. The RMS differences between the experimental measurements and analytical

predictions for the CAV hood face velocities were approximately 21% with no mannequin and 34% for the mannequin in place at 33% of sash opening. The results showed that the simulations agree with the experimental data reasonably well for both cases. The RMS error for the CAV case (with the mannequin) could be due to the chaotic and transient nature of the flow field in the wake region and the steady state time scheme was used. Similar to the nano hood, the velocity magnitude dropped significantly when the mannequin was present.

Hood interior airflow and particle dispersion patterns

The difference in the geometric design of both hoods resulted in different flow patterns inside the hoods.

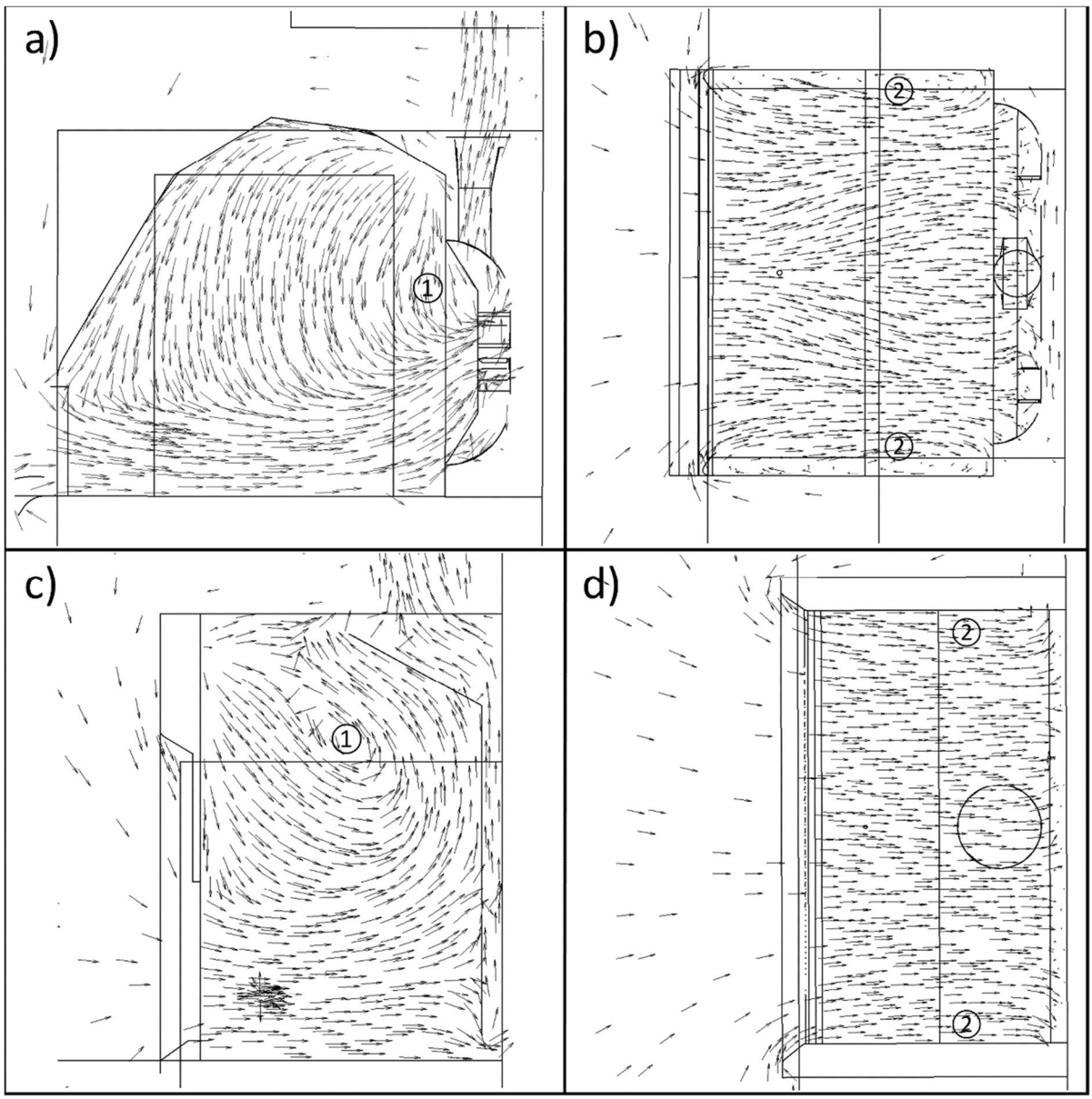

Fig. 3 Velocity at a) a vertical cross section of nano hood. b) A horizontal cross-section of nano hood. c) A vertical cross-section of CAV hood. d) A horizontal cross-section of CAV hood

Both hoods exhibited large recirculation zones behind the sash as air accelerates into the hood opening and then slows down when reaching the much larger hood volume (Fig. 3a and c, tag number 1). The existence of a recirculation region behind the sash has been found in these types of hoods by other researchers using experimental and numerical methods. The nano hood also exhibited secondary recirculation zones related to the side post airfoils, as shown in Fig. 3b. These side airfoils, which were meant to reduce turbulence inside the nano hood, generate a recirculation zone along the sides of the hood. This result may be surprising given that the side airfoil is small and intrudes into the hood space only a few centimeters. However, as the air is brought into the hood, these small airfoils greatly impact the flow patterns near the sides of the nano hood. The CAV hood flow pattern shows a much smaller side recirculation pattern primarily due to the fact that the side airfoils end flush with the sides of the hood and did not intrude into the hood space (see Fig. 3d, tag number 2).

To understand the performance of both designs on contaminant dispersion within the hood, a release of a tracer gas, SF_6, was simulated at the center of the hood and the predicted concentration contours at a vertical cross section are shown in Fig. 4 with and without a mannequin form in front of the hood. Figure 4a and b shows that the tracer gas gets caught up in the primary recirculation zone behind the nano hood sash but is reduced when the mannequin form is in front of the hood. However, Fig. 4c and d shows that the inclusion of the mannequin body in front of the CAV hood dramatically disturbs the flow field and causes the tracer gas to move towards the hood face and increases the tracer concentration in the primary recirculation zone behind the hood sash. This airflow dynamic may increase the risk of contaminant escape in the CAV hood when attended by an operator. Further the concentration of the tracer in the upper part of the hood, near the bottom of the hood sash, provides an opportunity for leakage of contaminants to easily reach the operator's breathing zone (see Figs. 4 and 6).

Effects of arm motion on hood containment

Simulations with both tracer gas and nanoparticle releases were conducted to better understand the impact of the withdrawal of arms from the hood on contaminant dispersion patterns. Figure 5 shows the impact of the highest withdrawal arm speed (2.5 m/s) on predicted tracer gas concentrations compared with no arm motion at a horizontal cut plane through the middle of the hood opening. The pulling arm motion does not seem to make a significant change in the dispersion patterns seen through this figure. However, the motion of the arm moving out of the hood shows that contaminant seems to be dragged out by the end of the arm (see Fig. 5b and d) and tends to enlarge the overall shape of the high SF_6 concentration zones to a minor degree. This action may increase the potential for dragging out tracer gas out of the hood near the hood face.

Table 2 contains a summary of the particle tracking results for a variety of simulation conditions, including varying source location (left, center, or right sphere location) and arm withdrawal speed (0, 0.5, 1.0, and 2.5 m/s). For all scenarios, more total particles were leaked from the CAV hood than the nano hood. Figure 6a–d shows the particle tracks released from a source at the side and in the center of the both the nano and CAV hoods. A large portion of particles entered into the primary recirculation zone before they were eventually cleared in the nano hood. The speed of arm pulling motion did not show a significant impact on particle trajectories for the nano case. On the contrary, only a small portion of particles entered into the primary recirculation zone as most particles were sucked directly into the lower opening of the baffle in the CAV hood, shown in Fig. 6c and d. When the arm removal speed increased, some particles started to reach the hood face and show a tendency to leak from the hood (Fig. 6d and Table 2). For the nano hood, only the highest arm removal rate resulted in loss of containment. These particles were predicted to escape the hood and move outward into the room. For the CAV hood, particles leaked at every condition even when there was no arm motion.

The airflow dynamics inside the hood coupled with the mannequin in front of the hood and the motion of the arms from the hood impacts the containment performance of these hoods. Further where sources are located within the hood and their proximity to the primary and secondary recirculation regions affects the potential for leakage. When the particles are released in the center of the hood downstream of the body, they are more efficiently captured and exhausted from the hood. In general,

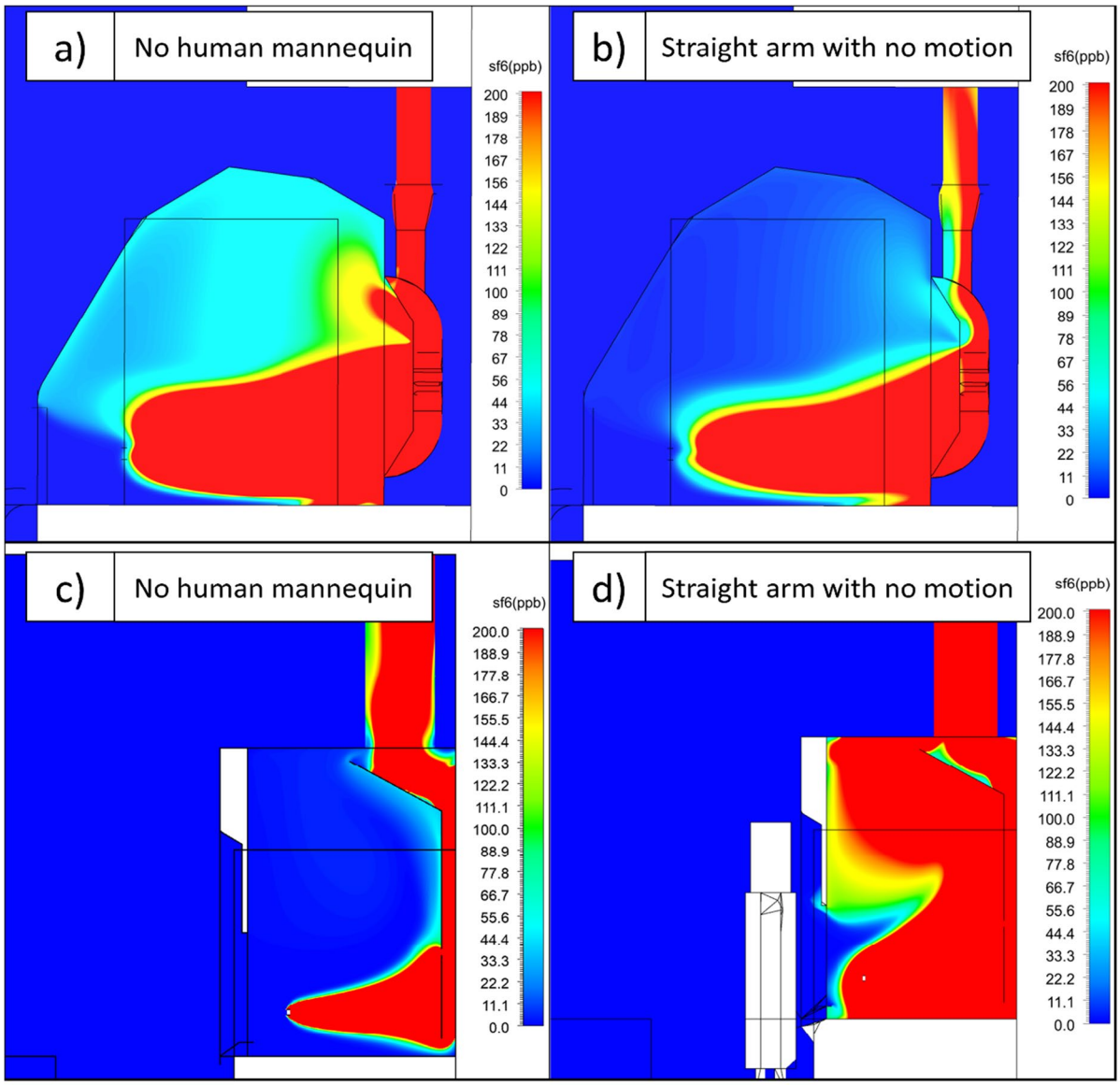

Fig. 4 SF_6 predicted concentration contours at a vertical cut plane with no human mannequin and with a straight-arm mannequin for a) nano hood without mannequin, b) nano hood with straight arm and no motion, c) CAV hood without mannequin, and d) CAV hood with straight arm and no motion. The concentration was measured in parts per billion (ppb)

with all simulations, particles become trapped in the recirculation zones resulting in some particles not being exhausted from the hood. Overall, both hoods leaked exhibited leakage of less than 1% based on these simulations (see Table 2); however, the nano hood showed less particle leakage than the CAV hood. Based on these results, the best containment condition is for the source to be located at the center of the hood, especially for the nano hood, which suffers from the side recirculation zones. When the contaminant is released inside the hood at the center, the average flow path is for the contaminant to be picked up and efficiently removed by either hood. However, when the contaminant is located near the side of the hood, the flow patterns inside the nano hood increase the potential for leakage as the streamlines released from a source near

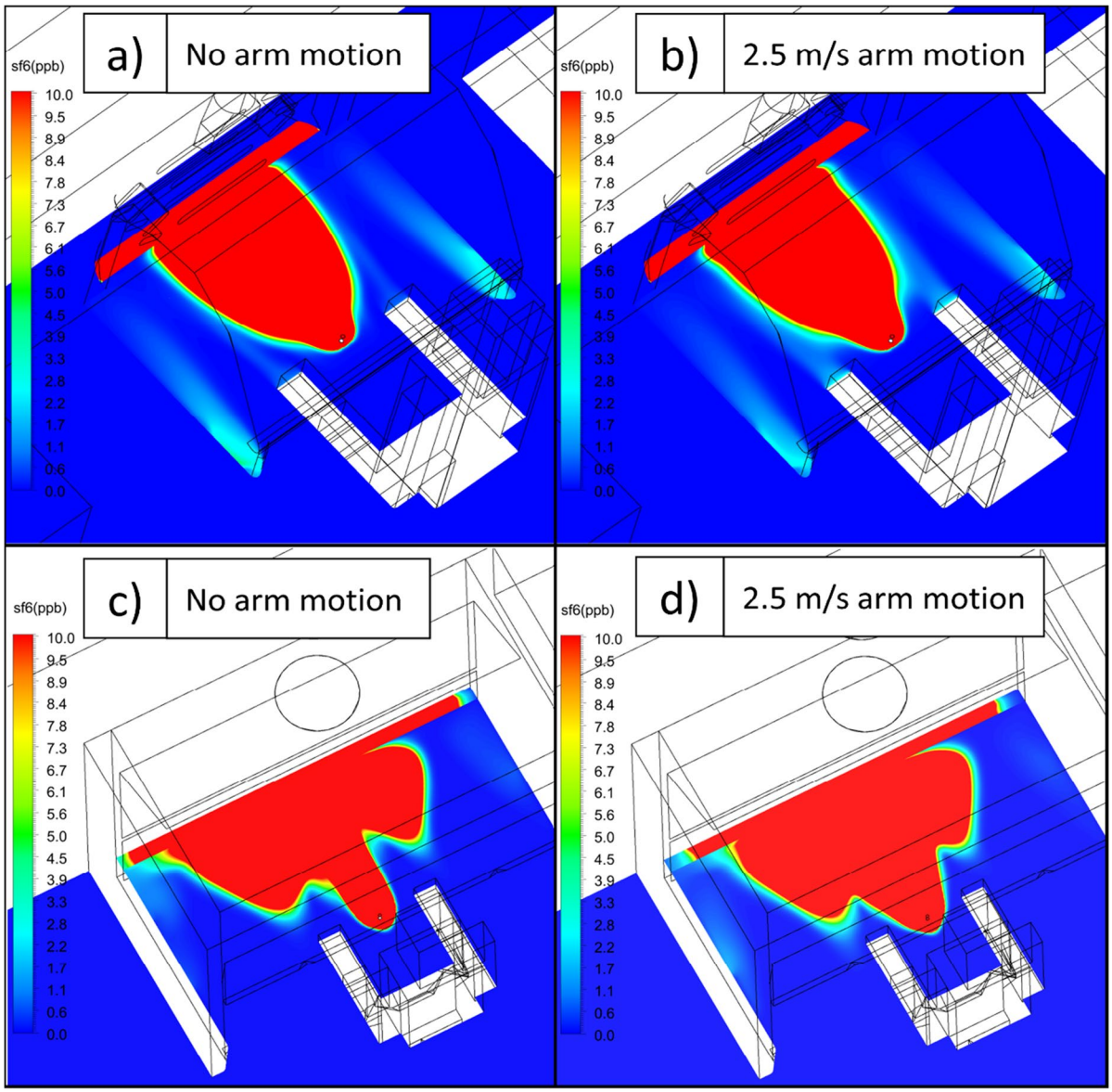

Fig. 5 SF_6 predicted concentration contours for the CAV hood with no arm motion and 2.5 m/s arm motion at a horizontal cut plane through both arms for a) nano hood with no arm motion, b) nano hood with 2.5 m/s arm motion, c) CAV hood with no arm motion, and d) CAV hood with 2.5 m/s arm motion. The concentration was measured in ppb

the side do not leave the hood space directly but move back towards the hood opening (see Fig. 6).

Discussion

The current study evaluated a new fume hood being marketed for the containment of nanomaterials during handling compared to an existing conventional fume hood. One of the key findings was that the the nano fume hood seemed to be less affected than the CAV hood by the presence of a body in front of the hood with the maximum opening face area allowed by the hood design. However, the use of aerodynamic features like the side airfoils, which intruded into the hood volume, created a secondary recirculation zone.

Table 2 Percentage (%) of 50 nm particles reaching hood face plane released under various simulation conditions including source location and arm withdrawal speeds for nano hood and traditional hood

Arm Withdrawal Speed (m/s)	Nano Hood				Traditional (CAV) Hood			
	Source Location				Source Location			
	Left	Center	Right	Total	Left	Center	Right	Total
0	0.008	0	0	0.008	0.012	0	0.014	0.026
0.5	0.051	0	0	0.051	0.041	0	0.039	0.080
1.0	0.064	0	0	0.064	0.050	0	0.090	0.140
2.5	0.092	0	0.014	0.106	0.202	0.005	0.136	0.343

Note: 56,589 particles were released for each location and simulation based on mesh size

This secondary recirculation zone interacted with the primary recirculation region behind the sash to trap contaminants increasing the potential for leakage. In smaller hoods, such as the nano hood evaluated (hood width of 86 cm versus mannequin width of 43 cm), the impact of these effects might be magnified since the worker's arms will more likely interact with the side recirculation zones. However, the results also indicate a potential re-design that might lead to an improvement of performance. Moving the side airfoils outside of the volume so that they terminate at the hood side should reduce the size of the side recirculation zone although the optimum inlet angle should be investigated using CFD and confirmed using flow visualization methodologies. For the CAV hood, the mannequin represented a far smaller blockage to the opening area since the hood width was approximately 1.5 times as large as the smaller nano hood. These factors as well as the design of the side airfoils resulted in better airflow patterns along the hood side.

For both hoods, as air enters the hood opening and slows down, a large recirculation region is created behind the sash. The presence of this recirculation zone (behind the sash) has been seen in research findings on fume hoods by many researchers (Tseng et al. 2006, 2010; Ljungqvist 1991; Hu et al. 1996, 1998; Nicholson et al. 2000; Lan and Viswanathan 2001a; Ivany et al. 1989). Complex turbulent airflow patterns arose in areas where the incoming air met a wall boundary—along the sides of the hood, at the work surface and along the bottom of the sash (Tseng et al. 2006). When a transient disturbance impacts these regions of the hood, contaminants inside the hood can leak out of the hood into the work environment. These disturbances may be due to many common sources including the presence and motion of the worker, room ventilation, sash movement, and the walk-by of workers within the room (Flynn and Ljungqvist 1995a, b; Huang et al. 2007a; Ljungqvist 1991, 1992; DiBerardinis et al. 1991a; Mosovsky 1995; Ahn et al. 2008; Caplan and Knutson 1982; Denev et al. 1997; Flynn et al. 1995). Huang et al. developed an air curtain hood which sought to address these design issues by changing the overall flow patterns associated with the hood (Huang et al. 2007b). In that design, an air jet emanates from the sash and forms a barrier to the potential for leakage of contaminants inside the hood. An evaluation of that hood during nanomaterial handling activities showed good containment performance (Tsai et al. 2010).

The presence of the mannequin did impact the airflow into the fume hood with a stagnation zone forming downstream of the mannequin. However, this factor was not sufficient to result in leakages for either hood. The impact of removing arms from the hood was evaluated with a Lagrangian particle tracking scheme. These simulations illustrated the effect of motion on the recirculation zones for both hoods which concentrate contaminants in the vortices behind the hood sash. For the nano hood, motion caused a much greater disturbance in the overall flow field inside the hood. This is likely due to the fact that the volumetric airflows are much lower for the nano hood than the CAV hood (nano hood: 2.83 m^3/min, CAV hood: 17.8 m^3/min). In addition, although the velocity at the face of both hoods were comparable for the simulation (nano hood: 0.36 m/s, CAV hood: 0.48 m/s), the air speeds decrease greatly once inside the nano hood as the air expands into the larger volume.

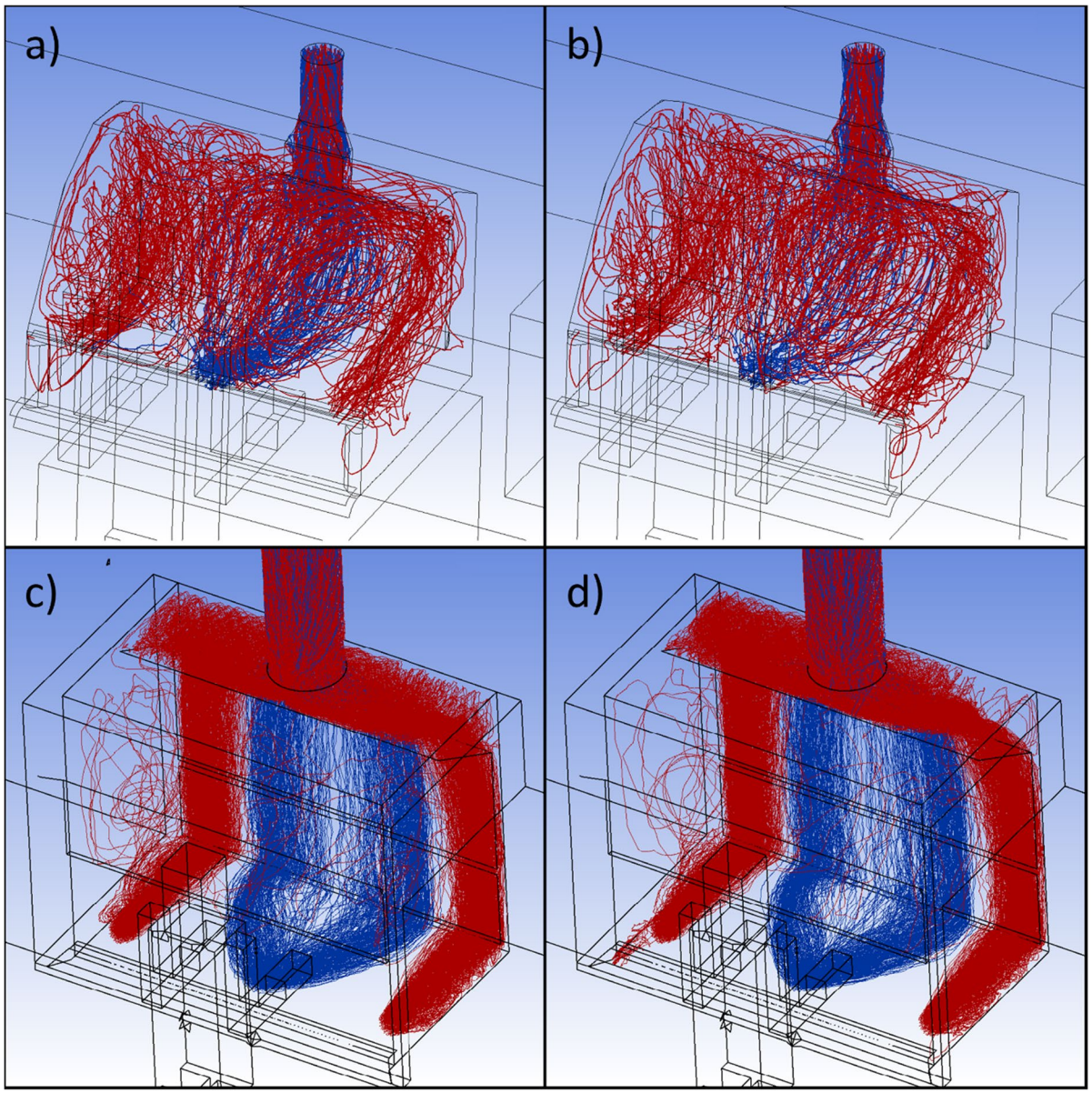

Fig. 6 Particle trajectories for the source at center of hood with a) nano hood with no arm motion. b) nano hood with 2.5 m/s arm motion. c) CAV hood with no arm motion and d) CAV hood with 2.5 m/s arm motion. The trajectories are colorized by red if they are released from the side source and blue if they are released from the center source

The procedure of removing the arm from the hood was demonstrated numerically through the steady state model. The flow pattern created by withdrawing the arms caused particles to be dragged out in the vicinity of the arm for the nano hood. This is consistent with fume hood experimental studies conducted by other researchers (Mosovsky 1995; DiBerardinis et al. 1991b). The leakage only occurred at the highest arm speed simulated and one that is higher than those likely performed by workers. However, this movement is conducted by every user upon completion of tasks, and overall leakage could certainly be increased if the user is also pulling out an object, such as a beaker which would further disturb the flow

field. The approach of using a moving wall boundary condition in a steady state framework is a reasonable initial approach that can be improved by using more recently available CFD techniques such as dynamic mesh methodologies.

With both the CAV and nano hood, the recirculation zones result in contaminants being transported to the front of the hood near the inlet boundary. As the particles get near the hood/room interface, the potential for leakage to occur increases due to user motion as well as outside disturbances, such as room air currents. These simulations did not include room air vents, which could have further disturbed the flow and resulted in leakage of particles from the hood. Other researchers have documented the negative impact of room air distribution on hood containment performance both experimentally and through numerical methods (Mosovsky 1995; Caplan and Knutson 1982; Denev et al. 1997; DiBerardinis et al. 1991b).

Finally, the airflow patterns in the hood were transient in nature as evidenced by the predicted tracer gas concentration results. As the flow was unsteady, there were limitations with using steady-state simulations. However, it was believed that the overall flow field features were well captured by the steady-state model, and agreement with experimental measurements validated this approach.

Conclusions

The dearth of published studies on the implementation and effectiveness of engineering controls for nanometer-sized particles such as engineered nanoparticles provide an opportunity to assess exposure control approaches. Many users have adopted the laboratory fume hood as the primary exposure control given its ubiquitous nature and history as a standard control used in most research laboratories. Some newly developed fume hoods introduced in the past decade are being specifically targeted for application in the nanotechnology and advanced material markets. This study illustrated limitations in one such design; similar hoods by other manufacturers may exhibit similar limitations. In addition, CFD was used to evaluate the potential impact of worker arm motion on containment effectiveness. Results of the modeling effort point to some commonsense approaches to minimizing the likelihood of arm motion resulting in worker exposure. Specifically, the operator could wait a prescribed amount of time before withdrawing their arms to allow for the clearance of nanoparticles and do so at a lower speed, as an improved work practice to minimize leakage and potential for exposure.

This study along, with others conducted, showed limitations of some fume hood containment test methods. These approaches include the need to utilize a mannequin when conducting tracer gas tests and to evaluate common worker maneuvers, such as removing their arms from the hood. In addition, hood containment assessment methods should collect data near each hood wall boundary since these areas represented the regions where leakage was most likely to occur. More research is required to address the issues at these boundaries where leakage may occur to gain a better understanding of the interaction between hood containment and room airflows.

Acknowledgements The authors acknowledge the financial support of the technical contract titled "Computational fluid dynamics analysis of ventilated enclosures for the handling of nanomaterials" provided by National Institute for Occupational Safety and Health (NIOSH) for this project. Dr. Kevin Dunn was supported by NIOSH for this manuscript.

The findings and conclusions in this manuscript are those of the authors and do not necessarily represent the official position of the National Institute for Occupational Safety and Health, Centers for Disease Control and Prevention. Mention of a specific product or company does not constitute endorsement by the National Institute for Occupational Safety and Health, Centers for Disease Control and Prevention.

Declarations

Conflict of interest The authors declare no competing interests.

References

Ahn K, Woskie S, DiBerardinis L, Ellenbecker M (2008) A review of published quantitative experimental studies on factors affecting laboratory fume hood performance. J Occup Environ Hyg 5(11):735–753. https://doi.org/10.1080/15459620802399989

ANSYS (2009) ANSYS FLUENT 12.0 Theory Guide

ASHRAE (2016) ANSI/ASHRAE standard 110-2016, methods of testing performance of laboratory fume hoods. ASHRAE, Inc., Atlanta

Asadi S, Bouvier N, Wexler A, Ristenpart W (2020) The coronavirus pandemic and aerosols: does COVID-19 transmit via expiratory particles? Aerosol Sci Technol 54(6):635–638

Bennett JS, Crouch KG, Shulman SA (2003) Control of wake-induced exposure using an interrupted oscillating jet. Am Ind Hyg Assoc J 64(1):24–29. https://doi.org/10.1080/15428110308984779

Bavasso I, Vilardi G, Stoller M, Chianese A, Di Palma L (2016) Perspectives in nanotechnology based innovative applications for the environment. Chem Eng 47

Braconnier R, Bonthoux F (2010) Fluid dynamics of cytotoxic safety cabinets. Ann Occup Hyg 54(2):236–246

Caplan KJ, Knutson GW (1982) Influence of room air supply on laboratory hoods. Am Ind Hyg Assoc J 43(10):738–746

Denev JA, Durst F, Mohr B (1997) Room Ventilation and Its Influence on the Performance of Fume Cupboards: A Parametric Numerical Study. Ind Eng Chem Res 36:458–466

DiBerardinis LJ, First MW, Ivany RE (1991a) Field Results of an in-place, quantitative performance test for laboratory fume hoods. Appl Occup Environ Hyg 6(3):227–231

DiBerardinis LJ, First MW, Ivany RE (1991b) Field Results of an in-place, quantitative perfromance test for laboratory fume hoods. Appl Occup Environ Hyg 6(3):227–231

Ding Y, Kuhlbusch TA, Van Tongeren M, Jiménez AS, Tuinman I, Chen R et al (2017) Airborne engineered nanomaterials in the workplace—a review of release and worker exposure during nanomaterial production and handling processes. J Hazard Mater 322:17–28

Dunn K, Tsai S, Woskie S, Bennett J, Garcia A, Ellenbecker M (2014) Evaluation of leakage from fume hoods using tracer gas, tracer nanoparticles and nanopowder handling test methodologies. J Occup Environ Hyg 11(10)

Flynn MR, Ljungqvist B (1995a) A review of wake effects on worker exposure. Ann Occup Hyg 39(2):211–221

Flynn MR, Ljungqvist B (1995b) A review of wake effects on worker exposure. Ann Occup Hyg 39:211–221

Flynn MR, Ahn K, Miller CT (1995) Three-dimensional finite-element simulation of a turbulent push-pull ventilation system. Ann Occup Hyg 39(5):573–589

George DK, Flynn MR, Goodman R (1990) The impact of boundary layer separation on local exhaust design and worker exposure. Appl Occup Environ Hyg 5(8):501–509

Hinds WC (1999) Aerosol technology - properties, behavior, and measurement of airborne particles. vol Book, Whole. Wiley-Interscience, New York

Hu P, Ingham DB, Wen X (1996) Effect of the location of the exhaust duct, an exterior obstruction and handle on the air flow inside and around a fume cupboard. Ann Occup Hyg 40(2):127–144

Hu P, Ingham DB, Wen X (1998) Effect of baffles and a louvered bypass on the airflow and the convective patterns of contaminant inside a fume hood. Am Ind Hyg Assoc J 59(5):303–312

Huang RF, Chen HD, Hung CH (2007a) Effects of walk-by and sash movement on contaminant leakage of air curtain-isolated fume hood. Ind Health 45(6):804–816

Huang RF, Wu YD, Chen HD, Chen CC, Chen CW, Chang CP et al (2007b) Development and evaluation of an air-curtain fume cabinet with considerations of its aerodynamics. Ann Occup Hyg 51(2):189–206. https://doi.org/10.1093/annhyg/mel051

Ivany RE, First MW, Diberardinis LJ (1989) A new method for quantitative, in-use testing of laboratory fume hoods. Am Ind Hyg Assoc J 50(5):275–280

Kim TH, Flynn MR (1991a) Airflow pattern around a worker in a uniform freestream. Am Ind Hyg Assoc J 52:287–296

Kim TH, Flynn MR (1991b) Modeling a worker's exposure from a hand-held source in a uniform freestream. Am Ind Hyg Assoc J 52(11):458–463

Kim TH, Flynn MR (1992) The effect of contaminant source momentum on a worker's breathing zone concentration in a uniform freestream. Am Ind Hyg Assoc J 53(12):757–766

Kulmala I, Saamanen A, Enbom S (1996) The effect of contaminant source location on worker exposure in the near-wake region. Ann Occup Hyg 40(5):511–523. https://doi.org/10.1016/0003-4878(96)00003-8

Lan NS, Viswanathan S (2001a) Numerical simulation of airflow around a variable volume/constant face velocity fume cupboard. AIHAJ 62(3):303–312

Lan NS, Viswanathan S (2001b) Numerical simulation of airflow around a variable volume/constant face velocity fume cupboard. Am Ind Hyg Assoc J 62(3):303–312

Ljungqvist B (1991) Aerodynamic design of fume cupboards. Safety Health Pract 8:36–40

Ljungqvist B (1992) Ventilated benches and enclosures in laboratories. Safety Health Pract 10:41–44

Mosovsky JA (1995) Sulfur hexafluoride tracer gas evaluations on hood exhaust reductions. Am Ind Hyg Assoc J 56(1):44–49

Nicholson GP, Clark RP, de Calcina-Goff ML (2000) Computational fluid dynamics as a method for assessing fume cupboard performance. Ann Occup Hyg 44(3):203–217

NIOSH (2009) Approaches to Safe Nanotechnology: Managing the Health and Safety Concerns Associated with Engineered Nanomaterials. Cincinnati, OH: US Department of Health and Human Services, Public Health Service, Centers for Disease Control and Prevention, National Institute for Occupational Safety and Health, DHHS (NIOSH) Publication No 2009–125

Ong S, Tan Y, Chia P, Lee T, Ng O, Wong M et al (2020) Air, surface environmental, and personal protective equipment contamination by severe acute respiratory syndrome coronavirus 2 (SARS-CoV-2) from a symptomatic patient. JAMA E1–E3. https://doi.org/10.1001/jama.2020.3227

Tsai SJ (2013) Potential inhalation exposure and containment efficiency when using hoods for handling nanoparticles. J Nanopart Res 15:1880. https://doi.org/10.1007/s11051-013-1880-2

Tsai SJ, Ada E, Isaacs J, Ellenbecker MJ (2009) Airborne nanoparticle exposures associated with the manual handling of nanoalumina and nanosilver in fume hoods. J Nanopart Res 11(1):147–161. https://doi.org/10.1007/s11051-008-9459-z

Tsai SJ, Huang RF, Ellenbecker MJ (2010) Airborne nanoparticle exposures while using constant-flow, constant-velocity, and air-curtain-isolated fume hoods. Ann Occup Hyg 54(1):78–87

Tseng L, Huang RF, Chen CC, Chang CP (2006) Correlation between airflow patterns and performance of a laboratory fume hood. J Occup Environ Hyg 3:694–706

Tseng LC, Huang RF, Chen CC, Chang CP (2007) Aerodynamics and performance verifications of test methods for laboratory fume cupboards. Ann Occup Hyg 51(2):173–187. https://doi.org/10.1093/annhyg/mel057

Tseng LC, Huang RF, Chen CC (2010) Significance of face velocity fluctuation in relation to laboratory fume hood performance. Ind Health 48(1):43–51

Varley JO, Ghorashi B (1997) The effect of turbulent structures on hood design—a review of CFD and flow visualization studies. HVAC R Res 3(3):291–308

Welling I, Andersson I-M, Rosen G, Räisänen J, Mielo T, Marttinen K et al (2000) Contaminant dispersion in the vicinity of a worker in a uniform velocity field. Ann Occup Hyg 44(3):219–225